Resolving the mesospheric nighttime 4.3 μm emission puzzle: New model calculations improve agreement with SABER observations

Peter A. Panka[1,2], Alexander A. Kutepov[2,3], Konstantinos S. Kalogerakis[4], Diego Janches[2], James M. Russell[5], Ladislav Rezac[6], Artem G. Feofilov[7], Martin G. Mlynczak[8], and Erdal Yiğit[1]

[1]Department of Physics and Astronomy, George Mason University, Fairfax, Virginia, USA.
[2]NASA Goddard Space Flight Center, Greenbelt, MD, USA.
[3]The Catholic University of America, Washington, DC, USA.
[4]Center for Geospace Studies, SRI International, Menlo Park, California, USA.
[5]Center for Atmospheric Sciences, Hampton University, Hampton, VA, USA.
[6]Max Planck Institute for Solar System Research, Göttingen, Germany.
[7]Laboratoire de Météorilogie Dynamique/IPSL/FX-Conseil, CNRS, Ecole Polytechnique, Université Paris-Saclay, 91128 Palaiseau, France.
[8]NASA Langley Research Center, Hampton, Virginia, USA.

Correspondence to: P. A. Panka (ppanka@masonlive.gmu.edu)

Abstract. Since 2002, SABER (Sounding of the Atmosphere using Broadband Emission Radiometry)/TIMED (Thermosphere, Ionosphere, Mesosphere, Energetics and Dynamics) has been continuously measuring the day- and nighttime infrared limb radiances of the mesosphere and lower thermoshere (MLT) in ten broadband channels. Recently, the MLT daytime temperature/pressure and CO_2 densities have been obtained self-consistently from SABER 15 μm and 4.3 μm emission observations. However, similar nighttime data remain unprocessed due to a lack of understanding of the 4.3 μm emission generating mechanisms. A previous study suggested the "direct" transfer $\mathrm{OH}(\nu) \Rightarrow \mathrm{N_2}(\nu) \Rightarrow \mathrm{CO_2}(\nu_3) \Rightarrow 4.3$ μm of vibrational excitation from OH(ν) to CO_2 in the nighttime mesosphere. However, accounting for this excitation mechanism **(with the currently accepted efficiency)** alone leads to significant under-prediction (by up to 80%) of observed 4.3 μm limb radiances. Recently, theoretical and laboratory studies have suggested an additional "indirect" nighttime channel $\mathrm{OH}(\nu) \Rightarrow \mathrm{O}(^1\mathrm{D}) \Rightarrow \mathrm{N_2}(\nu) \Rightarrow \mathrm{CO_2}(\nu_3) \Rightarrow 4.3$ μm of this energy transfer. We implemented this new channel in our non-LTE (non-Local Thermodynamic Equilibrium) model and show that, for various latitudinal and seasonal scenarios, including this additional channel brings differences between simulated and measured nighttime SABER 4.3 μm limb radiances to (-20, +30)%. These results confirm the important role of the new mechanism as a source of the nighttime 4.3 μm emission. This finding creates new opportunities for the application of CO_2 4.3 μm observations in the study of the energetics and dynamics of the nighttime MLT.

1 Introduction

The SABER (Sounding of the Atmosphere using Broadband Emission Radiometry) instrument on board the NASA TIMED (Thermosphere, Ionosphere, Mesosphere, Energetics and Dynamics) satellite (Russell III et al., 1999) measures the limb ra-

diance of the atmosphere in ten broadband infrared (IR) channels over an altitude range that spans the mesosphere and lower thermosphere (MLT). These measurements are aimed at retrieving various MLT parameters such as kinetic temperature, pressure, and densities of O_3, H_2O, CO_2, O, and other constituents.

Recently, daytime temperature/pressure and CO_2 densities have been obtained from the SABER 15 μm and 4.3 μm emission observations (Rezac et al., 2015) using a self-consistent two-channel retrieval approach which accounts for strong coupling between both emissions. Although CO_2 is one of the key trace constituents of the MLT, whose 15 μm emission is a main steady source of cooling in this region, up to now no observations of this constituent at nighttime are available. Additionally, CO_2 has a relatively long chemical lifetime, therefore, it can act as a tracer for dynamical transport processes, such as molecular and eddy diffusion, transport by atmospheric tides and also for determining the residual mean circulation. However, little is still known about its distribution and variability, particularly about its diurnal variation and its distribution in polar night. The extensive SABER nighttime 4.3 μm radiance observations, which are supposed to fill this knowledge gap, remain, however, still unprocessed due to a lack of understanding of physical mechanisms generating this emission. As a result, nighttime temperatures are currently retrieved independently from the SABER 15 μm channel radiances using day-night mean CO_2 densities from the WACCM (Whole Atmosphere Community Climate Model) model (Garcia et al., 2007).

A detailed study of nighttime 4.3 μm emissions was conducted in by López-Puertas et al. (2004) aimed at determining the dominant mechanisms of exciting $CO_2(\nu_3)$, where ν_3 is the asymmetric stretch mode that emits 4.3 μm radiation. The nighttime measurements of SABER channels 7 (4.3 μm), 8 (2.0 μm), and 9 (1.6 μm) for geomagnetically quiet conditions were analyzed, where channels 8 and 9 are sensitive to the OH ($\nu \leq$9) overtone radiation from levels ν = 8–9 and ν = 3–5, respectively. López-Puertas et al. (2004) showed a positive correlation between 4.3 μm and both OH channel radiances at a tangent height of 85 km. This correlation was associated with the transfer (Kumer et al., 1978) of energy of the vibrationally excited OH(ν) produced in the chemical reaction

$$H + O_3 \rightarrow O_2 + OH(\nu \leq 10) \tag{R1}$$

first to $N_2(1)$

$$OH(\nu \leq 10) + N_2(0) \leftrightarrow OH(\nu - 1) + N_2(1), \tag{R2}$$

and then further to $CO_2(\nu_3)$ vibrations

$$N_2(1) + CO_2(0) \leftrightarrow N_2(0) + CO_2(\nu_3) \tag{R3}$$

(hereafter "direct" mechanism). However, using laboratory rate coefficients of corresponding reactions the authors were unable to reproduce the 4.3 μm radiance observed by SABER. Although accounting for energy transfer from OH(ν) did provide a substantial enhancement to 4.3 μm emission, a 40% difference between simulated and observed radiance remained (for the SABER scan 22, orbit 01264, 77°N, 03 Mar 2002, which was studied in detail) for altitudes above 70 km. In order to fit measurements, on average, the authors found that 2.8-3 $N_2(1)$ molecules (instead of the **currently** accepted value of 1) are needed to be produced after each quenching of OH(ν) molecule in reaction (R2). Alternative excitation mechanisms that were

theorized to enhance the 4.3 μm radiance (i.e. via O_2 and direct energy transfer from OH to CO_2) were tested but found to be insignificant.

Recently, Sharma et al. (2015) suggested a new "indirect" mechanism of the OH vibrational energy transfer to $\mathbf{N_2}$**, i.e.** $\mathbf{OH}(\nu) \Rightarrow \mathbf{O}(^1\mathbf{D}) \Rightarrow \mathbf{N_2}(\nu)$**.** Accounting for this mechanism, but only considering OH(ν=9), these authors performed simple model calculations to validate its potential for enhancing mesospheric nighttime 4.3 μm emission from CO_2. They reported a simulated radiance enhancement between 18-55% throughout the MLT, which brought it closer to observed measurements. In a latest study, Kalogerakis et al. (2016) provided a definitive laboratory confirmation for the validity of this new mechanism.

Confining our consideration to quiet (non-auroral) nighttime conditions to avoid accounting for interactions between charged particles and molecules, whose mechanisms still remain poorly understood, we studied in detail the impact of both the "direct" mechanism alone and the combined effect of the two mechanisms on simulated nighttime SABER 4.3 μm radiances. We compared simulated radiances with the SABER measured radiances for various latitudes and seasons and present here results of this analysis.

2 Non-LTE Model Applied

A non-LTE analysis was applied to CO_2 and OH using the non-LTE ALI-ARMS (Accelerated Lambda Iterations for Atmospheric Radiation and Molecular Spectra) code package (Kutepov et al. (1998), Gusev and Kutepov (2003), Feofilov and Kutepov (2012)), which is based on the Accelerated Lambda Iteration approach (Rybicki and Hummer, 1991).

Our CO_2 non-LTE model is described in detail by Feofilov and Kutepov (2012). We modified its nighttime version to account for the "direct" mechanism, reactions (R1-R3), in a way consistent with that of López-Puertas et al. (2004) and added the "indirect" mechanism of Sharma et al. (2015) and Kalogerakis et al. (2016) as described in detail below. Our OH non-LTE model resembles that of Xu et al. (2012).

2.1 Model Inputs

Atmospheric pressure, temperature, O_3, O and H densities retrieved from SABER measurements (Remsberg et al. (2008), Smith et al. (2013), Mlynczak et al. (2013), Mlynczak et al. (2014), see also SABER data version 2.0 at http://saber.gats-inc.com) were used for simulating measured radiances in this study. The main atmospheric constituents (N_2 and O_2), as well as OH and CO_2 densities, were taken from the WACCM model (Garcia et al., 2007).

2.1.1 New Mechanism of $CO_2(\nu_3)$ excitation at nighttime

Sharma et al. (2015) suggested an additional mechanism that may contribute to the $CO_2(\nu_3)$ excitation at nighttime, and discussed in detail its available experimental and theoretical evidence. According to this mechanism, highly vibrationally excited OH(ν), produced by reaction (R1), rapidly loses several quanta of vibrational excitation in collisions with O(^{3}P) through a fast, spin-allowed, vibration-to-electronic energy transfer process that produces O(^{1}D),

$$\mathrm{OH}(\nu \geq 5) + \mathrm{O}(^3P) \leftrightarrow \mathrm{OH}(0 \leq \nu' \leq \nu - 5) + \mathrm{O}(^1D). \quad \text{(R4)}$$

Recently, Kalogerakis et al. (2016) have presented the first laboratory demonstration of this new OH(ν) + O(^{3}P) relaxation pathway.

The production at nighttime of electronically excited O(^{1}D) atoms in reaction (R4) has crucial importance. It triggers well known pumping mechanisms for daytime 4.3 μm emission (Nebel et al. (1994), Edwards et al. (1996)), where O(^{1}D) atoms are first quenched by collisions with N_2 in a fast spin-forbidden energy transfer process

$$O(^1D) + N_2(0) \leftrightarrow O(^3P) + N_2(\nu), \tag{R5}$$

then $N_2(\nu)$ transfers its energy to ground state N_2 via a very fast single quantum VV process

$$N_2(\nu) + N_2(0) \leftrightarrow N_2(\nu - 1) + N_2(1),$$

leaving N_2 molecules with an average of 2.2 vibrational quanta, which is followed by reaction (R3).

2.2 Collisional Rate Coefficients

We use, in our CO_2 non-LTE model, the same VT and VV collisional rate coefficients for the CO_2 lower vibrational levels as those of López-Puertas et al. (2004). However, a different scaling of these basic rates is applied for higher vibrational levels using the first-order perturbation theory as suggested by Shved et al. (1998).

The reaction rate coefficients applied in this study for modeling the transfer of OH(ν) vibrational energy to the $CO_2(\nu_3)$ mode are displayed in Table 1. The total chemical production rate of OH(ν) in reaction (R1) was taken from Sander et al. (2011) and the associated branching ratios for ν were taken from Adler-Golden (1997). The rate coefficient for reaction (R2) was taken from Adler-Golden (1997), measured at room temperature, and multiplied by a low temperature factor of 1.4 (Lacoursière et al., 2003) for MLT regions. **Following Sharma et al. (2015) and Kalogerakis et al. (2016) the rate coefficient of reaction (R4) for OH(ν=9) is (2.3$\pm$1)$\times 10^{-10}$ $\mathbf{cm^3 s^{-1}}$ for temperatures near 200 K.** In this study, we applied this coefficient for each OH($\nu \geq$5). Additionally, OH($\nu <$5) collisions with O(^{3}P) are considered completely inelastic and, therefore, we used for them the rate coefficient 3×10^{-11} $\mathrm{cm^3 s^{-1}}$ from Caridade et al. (2013). The rate coefficient for the reaction O(^{1}D) + N_2(0) (reaction (R5) in Table 1) was taken from Sander et al. (2011) with accounting for the fact that 33% of the electronic energy is transferred to N_2 (Slanger and Black, 1974) producing, on average, 2.2 N_2 vibrational quanta. The rate coefficient for the reaction OH($\nu \leq$10) + O_2(0) (reaction (R6) in Table 1) was taken from Adler-Golden (1997) and was scaled by a factor of 1.18 to account for MLT temperatures (Lacoursière et al. (2003),Thiebaud et al. (2010)).

3 Modeling Results

3.1 Vibrational Temperatures

The non-LTE population n_ν of a molecular vibrational level ν is usually described by its vibrational temperature, T_ν. From the Boltzmann formula,

$$\frac{n_\nu}{n_0} = \frac{g_\nu}{g_0} \exp[\frac{E_\nu - E_0}{kT_\nu}],$$

where T_ν is defined by the degree of excitation of level ν against the ground level 0 and g_ν and E_ν are the statistical weight and the energy of level ν, respectively. If T_ν=T_{kin} then level ν is in LTE.

Figure 1 shows the vibrational temperatures of the CO_2 levels of four isotopes, giving origin to 4.3 μm bands, which dominate the SABER nighttime signal (López-Puertas et al., 2004). These results were obtained for SABER scan 22, orbit 01264, 77°N, 03 March 2002. The same scan was used for the detailed analysis presented in the work by López-Puertas et al. (2004). The kinetic temperature retrieved for this scan from the SABER 15 μm radiances and vibrational temperature of $N_2(1)$ are also shown. Dashed and solid lines in Fig. 1 represent simulations with accounting for "direct" mechanism (reactions (R1-R3) alone) and with additionally implemented "indirect" mechanism (reaction (R4)), respectively.

Vibrational temperatures of CO_2 levels and $N_2(1)$ depart from LTE around 65 km. The additional accounting for reaction (R4) provides an increase of vibrational temperatures in the MLT. At 90 km, the T_ν of 626(00011) increases by 22 K, that of $N_2(1)$ increases by 26 K, whereas the minor isotopes (636, 628, and 627) and 626(01111) show a smaller enhancement of 3-8 K. In both simulations, CO_2(00011) of main isotope 626 and $N_2(1)$ have almost identical vibrational temperatures up to $\sim$87 km which is caused by an efficient VV exchange reaction (R3).

3.2 Comparison of Measured and Simulated Radiances

Figure 2 displays the measured SABER channel 7 (4.3 μm) radiance (black) for the scan described in Sect. 3.1. The violet curve in this figure represents the 4.3 μm simulated signal for this scan obtained by López-Puertas et al. (2004), long dash curve in Fig. 10 of this paper, with accounting for contribution in the channel 7 radiance emitted by OH($\nu \leq$10), and applying reactions (R1-R3) only ("direct" mechanism **with currently accepted efficiency 1**). Our calculations for this scan with accounting for "direct" mechanism alone are given by the blue curve. They also account for OH emission contribution and use inputs identical to those of (López-Puertas et al., 2004) except for OH densities. Whereas López-Puertas et al. (2004) retrieved OH densities from SABER measurements, OH for this and our calculations discussed below are taken from WACCM results (Garcia et al., 2007). Our calculations reproduce the result of (López-Puertas et al., 2004) very well between 70-95 km. There is a minor discrepancy around 87 km, where the OH peak resides, which is likely a result of OH density differences. Orange, red and green curves in Fig. 2 show results of our calculations with accounting for the combined effect of both "direct", reactions (R1-R3), and "indirect" reaction (R4) mechanisms. The three radiance profiles correspond to the range of rate coefficients reaction (R4) (see Table 1) within uncertainty limits estimated by Sharma et al. (2015). Accounting for the "indirect" mechanism "on top" of the "direct" one produces strong enhancement of 4.3 μm radiation for all runs in which the results display agreement to within (-23, +6.5)%, (-12, +10)%, and (-4, +20)% of SABER measurements, for rate coefficients 1.3, 2.3, and 3.3 $\times$ 10^{-10} $\mathrm{cm^3 sec^{-1}}$, respectively.

We also modeled 4.3 μm emissions for two representative nights (solar zenith angle (SZA) greater than 100°) at solstice, 15 July 2010 (311 scans), and equinox, 10 October 2008 (524 scans), which are shown in Fig. 3. The residual 4.3 μm radiance (simulated-measured)/measured is displayed with accounting for the "direct" mechanism alone (Fig. 3a and 3c) and when both "direct" and "indirect" mechanisms are included (Fig. 3b and 3d). Figures 3a and 3b display nighttime scans taken on 15 July 2010. When only the "direct" mechanism is considered (Fig. 3a), SABER measurements are reproduced to within

20% for southern latitudes and 30% for northern latitudes up to 75 km. Above 75 km, SABER measurements are shown to be gradually under-predicted from 30-80% for all latitudes, where the larger differences occur at higher altitudes. When both "direct" and "indirect" mechanisms are included (Fig. 3b), the simulated radiation is in agreement with SABER measurements to within (-10, +20)% for the majority of mid- and tropical latitudes above 90 km. Below 90 km for mid- and tropical latitudes, simulations predict SABER measurement to within (-20, +10)%. The "indirect" mechanism enhances radiances from 20% at 80 km to 80% at 100 km. For higher latitudes between 60°S and 80°S, simulated emission show good agreement with measurements up to 95 km. However, above 95 km, the 4.3 μm emissions are still under-predicted between 20% and 60%. This mismatched predictions may be hardly associated with any effects related to the geomagnetic activity since the kp index (<4) and the F10.7 index (=75) were low on this particular day. A more detailed investigation of this narrow altitude/latitude region is needed and will be performed in later studies.

Figures 3c and 3d display nighttime scans taken on 10 October 2008. Figure 3c shows agreement with SABER measurements to within 30% up to 75 km for all latitudes. Above 75 km, SABER measurements are shown to be gradually under-predicted from 40-70%, where percentages increase with higher altitudes. In the tropical regions, however, the disparity between simulated and SABER measurements is slightly greater at all altitudes compared to other regions. When both "direct" and "indirect" mechanisms are included (Fig. 3d), the simulated radiation is in agreement with SABER measurements to within (-20,+10)% for southern latitudes and (-10,+40)% for northern latitudes from 65-110 km. In both regions, radiance enhancements range from 20-30% below 80 km to up to 80-100% above 100 km. High atomic oxygen densities in some regions could be a result of the over-predictions for 4.3 μm emission modeling. In addition, unlike the solstice scans modeled in Fig. 3a and 3b, high latitude regions do not show any large under-predictions for equinox scenarios. Modeling emissions for alternative solstice and equinox nights, i.e. January and April, showed similar results as the nights modeled in Fig. 3.

Additionally, atomic oxygen densities retrieved by SABER have been reported to be at least 30% larger than other observations (Kaufmann et al., 2014). We found that lowering the atomic oxygen density by 50% reduces the 4.3 μm emission enhancement for all atmospheric scenarios, on average, by 5-20%, where the larger percentage differences occur at higher altitudes.

4 Discussion and Conclusions

Kumer et al. (1978) **first proposed the transfer of vibrational energy from chemically produced OH(ν) in the nighttime mesosphere to the $CO_2(\nu_3)$ vibration,** $\mathrm{OH}(\nu) \Rightarrow \mathrm{N}_2(\nu) \Rightarrow \mathrm{CO}_2(\nu_3)$. The effect of this mechanism on the SABER nighttime 4.3 μm **emission** was studied in detail by López-Puertas et al. (2004), who showed that in order to match observations , an additional enhancement is needed that would be equivalent to the production of 2.8-3 $N_2(1)$ molecules for each quenching reaction OH(ν)+N_2(0), **instead of the currently accepted one N_2(1) molecule**. López-Puertas et al. (2004) concluded that the required 30% efficiency in the OH(ν)+N_2(0) energy transfer "... is, in principle, possible, although the mechanism(s) whereby the energy is transferred is (are) not currently known".

Recently, Sharma et al. (2015) suggested a new **efficient** "indirect" channel of the OH(ν) energy transfer to the $\mathbf{N_2}(\nu)$ **vibrations,** $\mathbf{OH}(\nu) \Rightarrow \mathbf{O}(^1\mathbf{D}) \Rightarrow \mathbf{N_2}(\nu)$ and showed that it may provide an additional enhancement of the MLT nighttime 4.3 μm emission. Kalogerakis et al. (2016) provided a definitive laboratory confirmation **of this new OH(ν) + O vibrational relaxation pathway and measured its rate for OH(ν=9)+O. We added the new "indirect" OH(ν) + O energy transfer channel to the "direct" OH(ν) + N_2(0) mechanism (using the currently accepted efficiency of 1). Our non-LTE model of the nighttime CO_2 emissions assumes for the "indirect" channel a rate coefficient that is independent of the OH vibrational level.** We studied in detail the impact of **the combined "direct" and "indirect" mechanisms with** simulated SABER/TIMED nighttime 4.3 μm limb radiances and found that, while accounting for the "direct" mechanism alone leads to under-predicting the SABER measured radiances by up to 80%, **inclusion** of the new "indirect" channel in the model results in a significant reduction of these differences bringing them to (-20, +30)% for the majority of latitudes during equinox and solstice nights. This significant improvement suggests that the missing nighttime mechanism of $CO_2(\nu_3)$ pumping has finally been identified. **This confidence is based on the fact that the new mechanism accounts for most of the discrepancies for a large variety of atmospheric situations, leaving little room for other processes (that cannot be excluded, but are not expected to be significant).** Further improvements will require optimizing the set of rate coefficients used for OH(ν) relaxation by $O(^3P)$ and O_2 at mesospheric temperatures and, in particular, understanding the dependence of the indirect mechanism on the OH vibrational level. Relevant laboratory measurements and theoretical calculations are sorely needed to understand these relaxation rates and the quantitative details of the applicable mechanistic pathways. Nevertheless, the results presented here clearly demonstrate significant progress in understanding the mechanisms **of the nighttime excitation of N_2(1)** and generating the nighttime CO_2 4.3 μm emission, and represent an important step towards developing the algorithm(s) suitable for retrieving CO_2 densities in the MLT from the SABER nighttime limb radiances.

Acknowledgements. We would like to thank Ramesh Sharma for his helpful comments and productive collaboration with the new nighttime mechanism implementation. The work by P.A.P was supported by the NASA grant NNX14AN71G. The work by A.A.K. was supported by the NSF grant 1301762 and the NASA grant NNX15AN08G. The contributions of K.S.K were supported by NSF Grant 1441896.

References

Adler-Golden, S.: Kinetic parameters for OH nightglow modeling consistent with recent laboratory measurements, Journal of Geophysical Research, 102, 19 969–19 976, doi:10.1029/97JA01622, 1997.

Caridade, P. J. S. B., Horta, J.-Z. J., and Varandas, A. J. C.: Implications of the O+OH reaction in hydroxyl nightglow modeling, Atmospheric Chemistry and Physics, 13, 1–13, 2013.

Edwards, D. P., Kumer, J. B., López-Puertas, M., Mlynczak, M. G., Gopalan, A., Gille, J. C., and Roche, A.: Non-local thermodynamic equilibrium limb radiance near 10 μm as measured by UARS CLAES, Journal of Geophysical Research: Atmospheres, 101, 26 577–26 588, doi:10.1029/96JD02133, http://dx.doi.org/10.1029/96JD02133, 1996.

Feofilov, A. G. and Kutepov, A. A.: Infrared Radiation in the Mesosphere and Lower Thermosphere: Energetic Effects and Remote Sensing, Surveys in Geophysics, 33, 1231–1280, doi:10.1007/s10712-012-9204-0, http://link.springer.com/10.1007/s10712-012-9204-0, 2012.

Garcia, R. R., Marsh, D. R., Kinnison, D. E., Boville, B. A., and Sassi, F.: Simulation of secular trends in the middle atmosphere, 1950-2003, Journal of Geophysical Research Atmospheres, 112, 1–23, doi:10.1029/2006JD007485, 2007.

Gusev, O. A. and Kutepov, A. A.: Non-LTE Gas in Planetary Atmospheres, in: Stellar Atmosphere Modeling, edited by Hubeny, I., Mihalas, D., and Werner, K., vol. 288 of *Astronomical Society of the Pacific Conference Series*, pp. 318–330, 2003.

Kalogerakis, K. S., Matsiev, D., Sharma, R. D., and Wintersteiner, P. P.: Resolving the mesospheric nighttime 4.3 μm emission puzzle: Laboratory demonstration of new mechanism for OH(υ) relaxation, Geophysical Research Letters, doi:10.1002/2016GL069645, http://doi.wiley.com/10.1002/2016GL069645, 2016.

Kaufmann, M., Zhu, Y., Ern, M., and Riese, M.: Global distribution of atomic oxygen in the mesopause region as derived from SCIAMACHY O(^{1}S) green line measurements, Geophysical Research Letters, 41, 6274–6280, doi:10.1002/2014GL060574, http://dx.doi.org/10.1002/2014GL060574, 2014.

Kumer, J. B., Stair, Jr., A. T., Wheeler, N., Baker, K. D., and Baker, D. J.: Evidence for an $OH^{\neq vv} \rightarrow N_2^{\neq vv} \rightarrow CO_2(\nu_3) \rightarrow CO_2 + h\nu$ (4.3 μm) Mechanism for 4.3-μm Airglow, Journal of Chemical Physics, 83, 4743–4747, 1978.

Kutepov, A. A., Gusev, O. A., and Ogibalov, V. P.: Solution of the Non-LTE Problem for Molecular Gas in Planetary Atmospheres: Superiority of Accelerated Lambda Iteration, Journal of Quantitative Spectroscopy and Radiative Transfer, 60, 199–220, 1998.

Lacoursière, J., Dyer, M. J., and Copeland, R. A.: Temperature dependence of the collisional energy transfer of OH(v=10) between 220 and 310 K, Journal of Chemical Physics, 118, 1661–1666, doi:10.1063/1.1530581, 2003.

López-Puertas, M., Garcia-Comas, M., Funke, B., Picard, R. H., Winick, J. R., Wintersteiner, P. P., Mlynczak, M. G., Mertens, C. J., Russell III, J. M., and Gordley, L. L.: Evidence for an OH(ν) excitation mechanism of CO_2 4.3 μm nighttime emission from SABER/TIMED measurements, Journal of Geophysical Research, 109, 2–15, doi:10.1029/2003JD004383, 2004.

Mlynczak, M. G., Hunt, L. A., Mast, J. C., Thomas Marshall, B., Russell, J. M., Smith, A. K., Siskind, D. E., Yee, J.-H., Mertens, C. J., Javier Martin-Torres, F., Earl Thompson, R., Drob, D. P., and Gordley, L. L.: Atomic oxygen in the mesosphere and lower thermosphere derived from SABER: Algorithm theoretical basis and measurement uncertainty, Journal of Geophysical Research: Atmospheres, 118, 5724–5735, doi:10.1002/jgrd.50401, http://doi.wiley.com/10.1002/jgrd.50401, 2013.

Mlynczak, M. G., Hunt, L. A., Marshall, B. T., Mertens, C. J., Marsh, D. R., Smith, A. K., Russell, J. M., Siskind, D. E., and Gordley, L. L.: Atomic hydrogen in the mesosphere region derived from SABER: Algorithm theoretical basis, measurement uncertainty, and results, Journal of Geophysical Research: Atmospheres, 119, 3516–3526, doi:10.1002/2013JD021263, 2014.

Nebel, H., Wintersteiner, P. P., Picard, R. H., Winick, J. R., and Sharma, R. D.: CO_2 non-local thermodynamic equilibrium radiative excitation and infrared dayglow at 4.3 μm: Application to Spectral Infrared Rocket Experiment data, Journal of Geophysical Research: Atmospheres, 99, 10 409–10 419, doi:10.1029/94JD00315, http://dx.doi.org/10.1029/94JD00315, 1994.

Remsberg, E. E., Marshall, B. T., Garcia-Comas, M., Krueger, D., Lingenfelser, G. S., Martin-Torres, J., Mlynczak, M. G., Russell, J. M., Smith, A. K., Zhao, Y., Brown, C., Gordley, L. L., Lopez-Gonzalez, M. J., Lopez-Puertas, M., She, C. Y., Taylor, M. J., and Thompson, R. E.: Assessment of the quality of the version 1.07 temperature-versus-pressure profiles of the middle atmosphere from TIMED/SABER, Journal of Geophysical Research Atmospheres, 113, 1–27, doi:10.1029/2008JD010013, 2008.

Rezac, L., Kutepov, A., Russell III, J. M., Feofilov, A. G., Yue, J., and Goldberg, R. A.: Simultaneous retrieval of T(p) and CO_2 VMR from two-channel non-LTE limb radiances and application to daytime SABER/TIMED measurements, Journal of Atmospheric and Solar-Terrestrial Physics, 130-131, 23–42, doi:10.1016/j.jastp.2015.05.004, http://linkinghub.elsevier.com/retrieve/pii/S1364682615000954, 2015.

Russell III, J. M., Mlynczak, M. G., Gordley, L. L., Tansock, Jr., J. J., and Esplin, R. W.: Overview of the SABER experiment and preliminary calibration results, Proc. SPIE, 3756, 277–288, doi:10.1117/12.366382, http://dx.doi.org/10.1117/12.366382, 1999.

Rybicki, G. B. and Hummer, D. G.: An accelerated lambda iteration method for multilevel radiative transfer. I - Non-overlapping lines with background continuum, Astronomy and Astrophysics, 245, 171–181, 1991.

Sander, S. P., Abbatt, J., Barker, J. R., Burkholder, J. B., Friedl, R. R., Golden, D. M., Huie, R. E., Kolb, C. E., Kurylo, M. J., Moortgat, G. K., Orkin, V. L., and Wine, P. H.: Chemical Kinetics and Photochemical Data for Use in Atmospheric Studies, Evaluation Number 17, JPL Publication 10-6, pp. 1–684, http://jpldataeval.jpl.nasa.gov/, 2011.

Sharma, R. D., Wintersteiner, P. P., and Kalogerakis, K. S.: A new mechanism for OH vibrational relaxation leading to enhanced CO_2 emissions in the nocturnal mesosphere, Geophysical Research Letters, 42, 4639–4647, doi:10.1002/2015GL063724, 2015.

Shved, G. M., Kutepov, A. A., and Ogibalov, V. P.: Non-local thermodynamic equilibrium in CO_2 in the middle atmosphere. I. Input data and populations of the ν_3 mode manifold states, Journal of Atmospheric and Solar-Terrestrial Physics, 60, 289–314, doi:10.1016/S1364-6826(97)00076-X, 1998.

Slanger, T. G. and Black, G.: Electronic-to-vibrational energy transfer efficiency in the $O(^1D)$-N_2 and singlet $O(^1D)$-CO systems, J. Chem. Phys, 60, 468–477, doi:10.1063/1.1681064, 1974.

Smith, A., Harvey, V., Mlynczak, M. G., Funke, B., García-Comas, M., Hervig, M., Kaufmann, M., Kyrölä, E., López-Puertas, M., McDade, I., et al.: Satellite observations of ozone in the upper mesosphere, Journal of Geophysical Research: Atmospheres, 118, 5803–5821, 2013.

Thiebaud, J. E., Copeland, R. A., and Kalogerakis, K. S.: Vibrational Relaxation of OH(ν = 7) with O, O_2, and H, Abstract #SA43A-1752, American Geophysical Union Fall Meeting, San Francisco, CA, 2010.

Xu, J., Gao, H., Smith, A. K., and Zhu, Y.: Using TIMED/SABER nightglow observations to investigate hydroxyl emission mechanisms in the mesopause region, Journal of Geophysical Research: Atmospheres, 117, 1–22, doi:10.1029/2011JD016342, 2012.

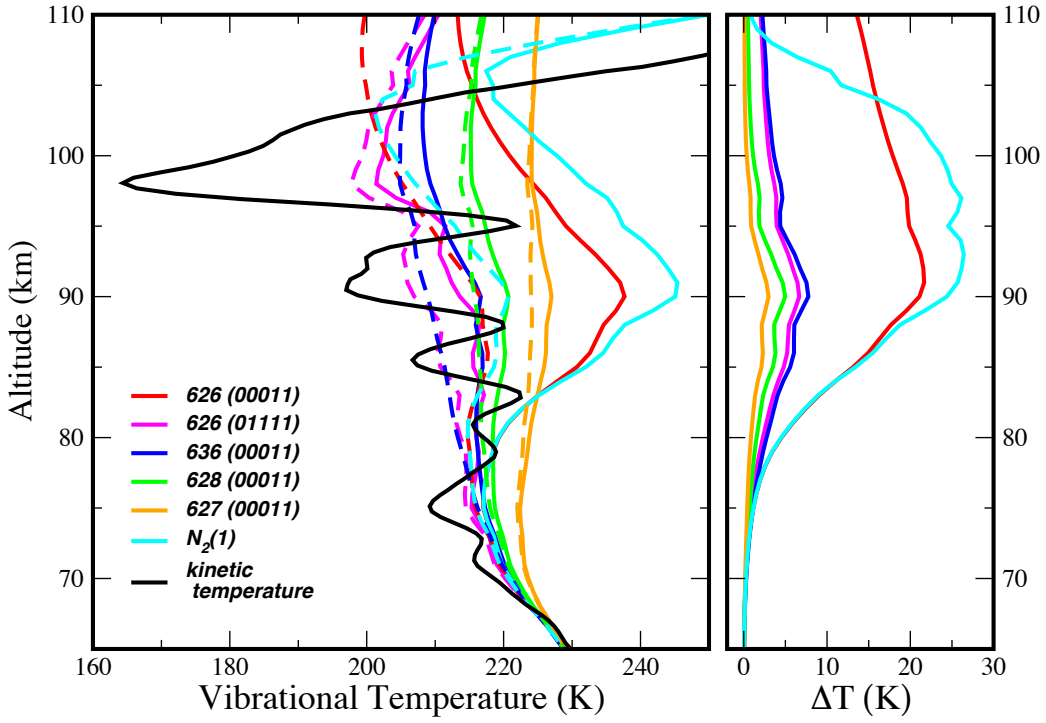

Figure 1. Nighttime vibrational temperatures of CO_2(00011) of four CO_2 isotopes, CO_2(01111) of main CO_2 isotope, and of N_2(1) for SABER scan 22, orbit 01264, 77°N, 03 March 2002. Left: dashed lines - no reaction (R4); solid lines - with reaction (R4) included, k_4=2.3×10^{-10} cm^3s^{-1}. Right: vibrational temperature differences.

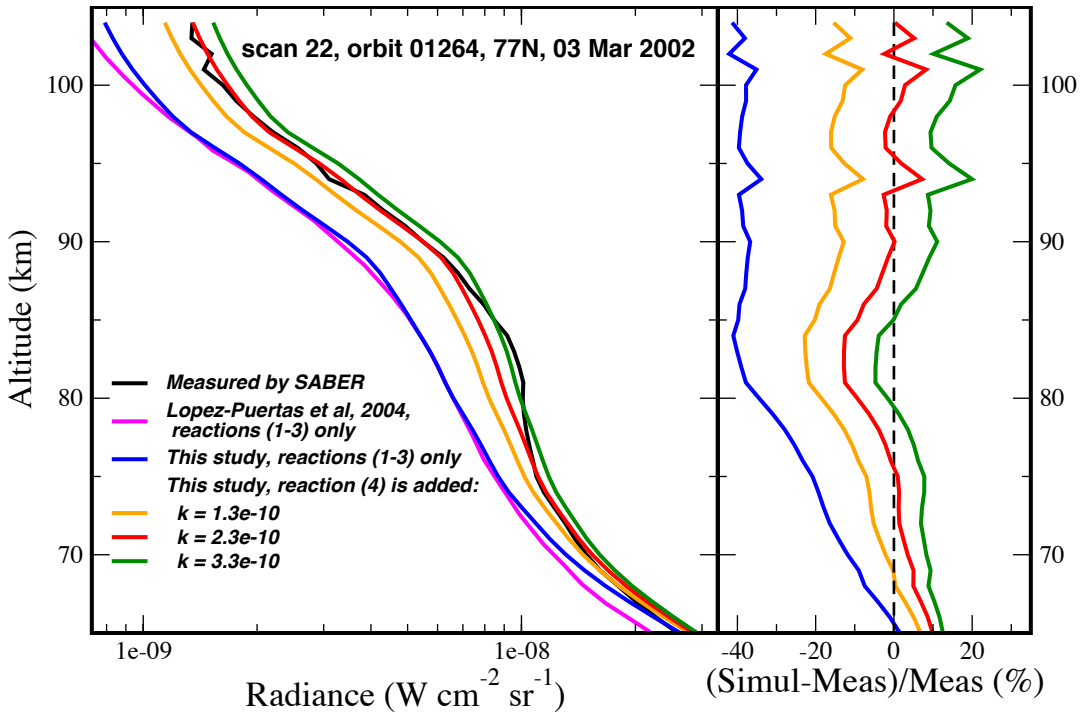

Figure 2. Left: measured and simulated SABER nighttime radiances in channel 7 (4.3 μm) for SABER scan 22, orbit 01264, 77°N, 03 March 2002. SABER measured (black); from López-Puertas et al. (2004), only reactions (R1-R3) included (violet); this study, only reactions (R1-R3) included (blue); this study, reaction (R4) added with k_4=1.3×10^{-10} cm^{3}s^{-1} (orange), k_4=2.3×10^{-10} cm^{3}s^{-1} (red), k_4=3.3×10^{-10} cm^{3}s^{-1} (green). Right: radiance relative difference (simulated-measured)/measured in percent.

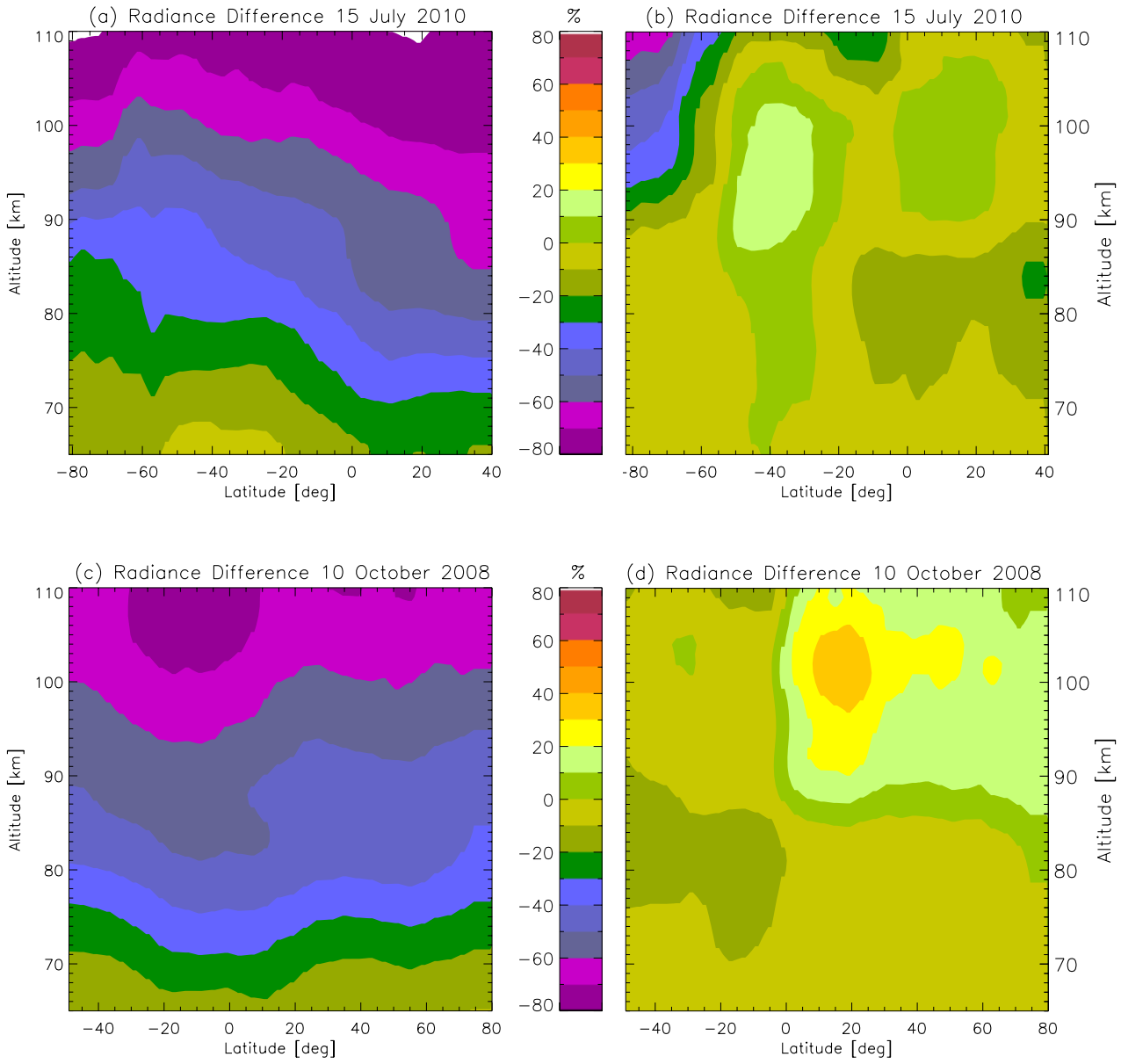

Figure 3. Residual CO_2 4.3 μm radiance (simulated-measured)/measured. (a): without and (b): with new "indirect" mechanism (using k_4=2.3$\times 10^{-10}$ $cm^3 s^{-1}$ for reaction (R4)) suggested by Sharma et al. (2015) for all nighttime scans on 15 July 2010; (c and d): same for all nighttime scans on 10 October 2008.

Table 1. Significant collisional processes used in model

	Reaction	Reaction Rate ($\mathrm{cm^3 sec^{-1}}$)	Reference
(R1)	$H + O_3 \leftrightarrow OH(\nu \leq 10) + O_2$	$k_1 = f_\nu^a \times 1.4 \times 10^{-10} \exp(-470/T)$	Sander et al. (2011) & Adler-Golden (1997)
(R2)	$OH(\nu \leq 10) + N_2(0) \leftrightarrow OH(\nu\text{-}1) + N_2(1)$	$k_2 = f_\nu^b \times 1.4 \times 10^{-13}$	Adler-Golden (1997) & Lacoursière et al. (2003)
(R3)	$N_2(1) + CO_2(0) \leftrightarrow N_2(0) + CO_2(\nu_3)$	$k_3 = 8.91 \times 10^{-12} \times T^{-1}$	Shved et al. (1998)
(R4)	$OH(\nu \geq 5) + O(^3P) \leftrightarrow OH(0 \leq \nu' \leq \nu\text{-}5) + O(^1D)$	$k_4 = (2.3 \pm 1) \times 10^{-10}$	Kalogerakis et al. (2016) & Sharma et al. (2015)
	$OH(\nu < 5) + O(^3P) \leftrightarrow OH(0) + O(^3P)$	$k_4 = 3 \times 10^{-11}$	Caridade et al. (2013)
(R5)	$O(^1D) + N_2(0) \leftrightarrow O(^3P) + N_2(\nu)$	$k_5 = 2.15 \times 10^{-11} \exp(110/T)$	Sander et al. (2011)
(R6)	$OH(\nu \leq 10) + O_2(0) \leftrightarrow OH(\nu) + O_2(1)$	$k_6 = f_\nu^c \times 1.18 \times 10^{-13}$	Adler-Golden (1997)

[a] $f_\nu(\nu\text{=}5\text{-}9) = (0.01, 0.03, 0.15, 0.34, 0.47)$

[b] $f_\nu(\nu\text{=}1\text{-}10) = (0.06, 0.10, 0.17, 0.30, 0.52, 0.91, 1.6, 7, 4.8, 6)$

[c] $f_\nu(\nu\text{=}1\text{-}10) = (1.9, 4, 7.7, 13, 25, 43, 102, 119, 309, 207)$